# Depth-resolved measurement of ocular fundus pulsations by low-coherence tissue interferometry

**Nikolaus Dragostinoff**
**René M. Werkmeister**
Medical University of Vienna
Center for Biomedical Engineering and Physics
Währinger Strasse 13
Vienna 1090
Austria

**Martin Gröschl**
Vienna University of Technology
Institut für Allgemeine Physik
Wiedner Hauptstrasse 8-10/134
Vienna 1040
Austria

**Leopold Schmetterer**
Medical University of Vienna
Center for Biomedical Engineering and Physics
Währinger Strasse 13
Vienna 1090
Austria
    and
Department of Clinical Pharmacology
Währinger Gürtel 18-20
Vienna 1090
Austria

**Abstract.** A device that allows for the measurement of ocular fundus pulsations at preselected axial positions of a subject's eye is presented. Unlike previously presented systems, which only allow for observation of the strongest reflecting retinal layer, our system enables the measurement of fundus pulsations at a preselected ocular layer. For this purpose the sample is illuminated by light of low temporal coherence. The layer is then selected by positioning one mirror of a Michelson interferometer according to the depth of the layer. The device contains a length measurement system based on partial coherence interferometry and a line scan charge-coupled device camera for recording and online inspection of the fringe system. *In-vivo* measurements in healthy humans are performed as proof of principle. The algorithms used for enhancing the recorded images are briefly introduced. The contrast of the observed interference pattern is evaluated for different positions of the measurement mirror and at various distances from the front surface of the cornea. The applications of such a system may be wide, including assessment of eye elongation during myopia development and blood-flow-related changes in intraocular volume. © *2009 Society of Photo-Optical Instrumentation Engineers.* [DOI: 10.1117/1.3251049]

## 1 Introduction

The measurement of fundus pulsations (i.e., distance variations between cornea and retina during the cardiac cycle) has been used for the study of various ocular diseases, which are associated with alterations in choroidal blood flow, such as age-related macular degeneration, glaucoma, and diabetic retinopathy, and for the study of the influence of several vasoactive drugs on ocular blood circulation.[1–7] Choroidal blood vessels are difficult to access because they are located behind the outer retina. Different techniques were proposed to gain insight into choroidal blood flow based on angiography,[8] laser Doppler flowmetry,[9] pneumotonometry,[10] and color Doppler imaging of the posterior ciliary arteries.[11] We have introduced fundus pulsation measurement based on a laser interferometric method. In previously presented systems, the eye is illuminated by a collimated laser beam of long coherence length.[12,13] Part of the light is reflected at the front surface of the cornea, another part at the fundus. Due to a phenomenon called fundus pulsation, which is described in detail later, the distance between the front surface of the cornea and the retina changes with the heart cycle. These two reflected waves generate concentric circular interference fringes, which are imaged onto a linear charge-coupled device (CCD) array. The

signal of the CCD array is recorded over time, resulting in a so-called synthetic interferogram covering information on the time course of changes in corneo-retinal distance. The maximum distance change during the cardiac cycle is called fundus pulsation amplitude (FPA). The reflection from the posterior segment most likely occurs from the retinal pigment epithelium or Bruch's membrane.[5] Only the interferogram resulting from the strongest reflection of the posterior pole is visible. Whereas other interferogram systems may also arise from other retinal interfaces, they are not visible.

Based on this approach we have shown that the phenomenon of fundus pulsation results from the rhythmic filling of the choroid during the cardiac cycle. During systole the blood flow entering the eye exceeds the blood flow leaving the eye through the ocular veins. Hence, the choroid engorges, associated with a slight protrusion of the retinal structures toward the cornea and an outward movement of the sclera due to an increase in intraocular volume. Whereas the former can be measured with laser interferometry, the latter cannot be quantified by any means to date. Relying on a mathematical model of the choroid, we were able to obtain realistic measures of choroidal blood flow in humans based on FPA measurements.[14] The change in ocular volume during the cardiac cycle is associated with a change in intraocular pressure.[10] We have shown that there is a high degree of correlation between the pulse amplitude of this intraocular pres-

Address all correspondence to: Leopold Schmetterer, Medical University of Vienna, Center for Biomedical Engineering and Physics, Währinger Strasse 13, Vienna, 1090, Austria. Tel: 43-1404002981; Fax: 43-1404002998; E-mail: leopold.schmetterer@meduniwien.ac.at
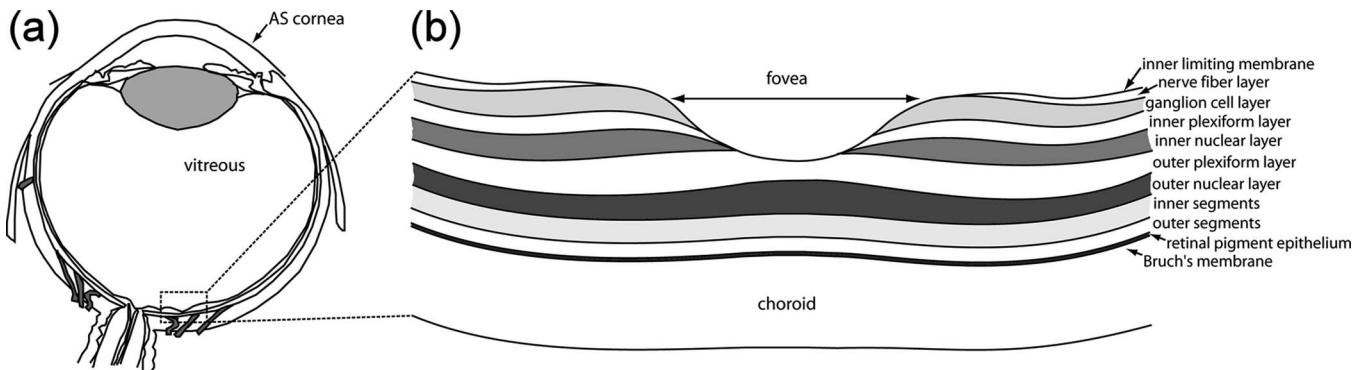
**Fig. 1** Schematic diagram of (a) the human eye with (b) the main layers in the posterior segment of the eye. AS is the anterior surface of the cornea.

sure change and the FPA in healthy young emmetropic subjects.[5,15,16] In addition, we have shown that there is an association between FPA and the pulsatile ocular blood flow (POBF), as calculated from the time course of the intraocular pressure changes.[5,15,16]

One problem with the calculation of POBF from laser interferometric data is associated with the fact that distance changes between the anterior surface of the cornea and the submacular sclera cannot be measured.[14] We introduce an approach called low-coherence tissue interferometry (LCTI), which allows us to measure distance changes between the cornea and preselected reflecting interfaces at the posterior pole of the eye, such as different retinal and choroidal layers in human subjects (see Fig. 1 for a schematic diagram), and furthermore, scleral structures in animal experiments.

## 2 Principles of Low-Coherence Tissue Interferometry

The use of short coherent light for imaging purposes has gained wide application in ophthalmology. The measurement of the eye length as well as the determination of intraocular distances are based on partial coherence interferometry (PCI) using light of high spatial coherence, but low temporal coherence.[17–20] Applications of this technique *in vivo* have been reported for measuring the length of the human eye.[21,22] This technique forms the basis of the commercially available IOL master (Zeiss, Jena, Germany) for the measurement of axial eye length.

For illumination, a superluminescent diode (SLD) with short coherence length $l_c$ is used. The beam is split by an external Michelson interferometer with unequal arm lengths into two components, which have a path difference equal to twice the arm length difference of the interferometer. The two beams illuminating the eye are reflected at the cornea and at the various layers of the fundus. If one of the intraocular distances equals (within $l_c$) the path difference, the beams reflected at the respective interfaces will interfere.

One of the mirrors of the Michelson interferometer is mounted on a stepper motor and moved at a constant speed $v$. The Doppler shift of the corresponding beam due to this movement is $f_D = 2v/\lambda$. Thus, the superposition of the two beams is modulated by $f_D$. The beams are focused onto a photodetector [avalanche photodiode (APD)]. This signal is amplified and filtered by a bandpass filter with a central fre-

quency of $f_D$. The envelope of the signal is recorded by a data acquisition card (DAC) as a function of the position of the stepper motor (which corresponds to the arm length difference $d$ of the Michelson interferometer), resulting in a curve called an optical A-scan. From the positions of the signal peaks in an A-scan, the respective optical intraocular distances can be obtained directly. The resolution that can be achieved by this technique is of the order of $l_c$. For a Gaussian-shaped spectrum, the coherence length (in air) can be calculated by:

$$l_c = \frac{2 \ln 2}{\pi} \frac{\lambda_0^2}{\Delta\lambda}, \qquad (1)$$

where $\lambda_0$ is the central wavelength and $\Delta\lambda$ the full width at half maximum (FWHM) bandwidth of the light source. The advantage of the dual-beam PCI technique for the measurement of eye length is the elimination of the effects of longitudinal eye motions.[17–20]

The basic idea of LCTI is to combine the principles of PCI and fundus pulsation measurement. In the previously presented approach to measure fundus pulsations,[13] the eye is illuminated by a collimated laser beam of high coherence length with a wavelength of 783 nm. The beam is reflected at the front surface of the cornea and at the retina. The wave originating from the front surface of the cornea is close to spherical, while the wave reflected from the fundus is plane. Therefore the two waves generate nonlocalized concentric circular interference fringes.[5] The maximum contrast of the interference pattern is approximately 30 to 40 mm in front of the eye, depending on the test subject. A distance variation between cornea and retina causes a change in interference order $\Delta N(t)$, which can be determined by counting the fringes moving through a fixed point. The change in optical distance $\Delta L(t)$ can then be calculated by $\Delta L(t) = \Delta N(t) * \lambda/2$, allowing for the calculation of the FPA.

The plane of maximum contrast is imaged by a lens onto a linear CCD, which is positioned in the center of the interference fringes. Each readout of the CCD array is captured by a personal computer (PC) and plotted along the time axis, resulting in a synthetic interferogram. By counting the fringes moving inward and outward, the change of interference order $\Delta N$ can be drawn as a function of time resulting in a contraction-dilatation graph.
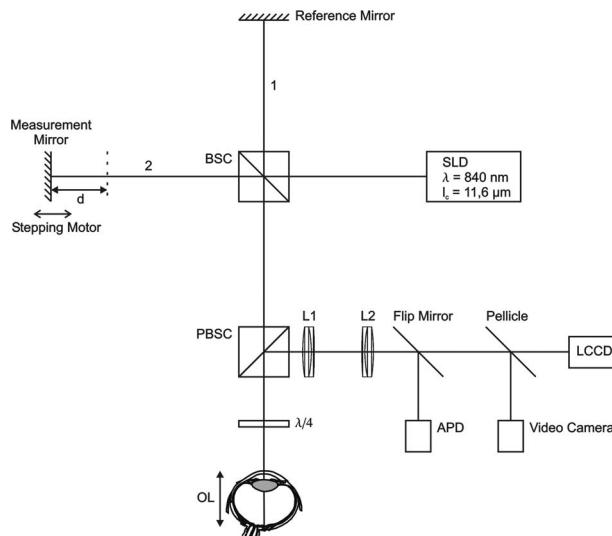
**Fig. 2** Optical setup: SLD, super luminescent diode; BSC, beamsplitter cube; PBSC, polarizing beamsplitter cube; APD, avalanche photo diode; and LCCD, linear CCD array. Depth ranging is provided by a scanning mirror.

To allow for measurements of time-resolved distance changes between the front surface of the cornea and preselected retinal layers, the following approach is employed. LCTI comprises a PCI system for the measurement of axial eye length. In the detection arm, an additional beamsplitter is introduced and part of the light is directed toward a CCD array, whereas the other part of the light is directed toward the APD for the measurement of intraocular distances. This allows for real-time assessment of tissue pulsations as long as the optical distances between the two interferometer arms and the optical distance between the two ocular surfaces are within the coherence length of the light source. Hence, the corresponding layer is preselected by the position of the mirrors within the Michelson interferometer.

The measurement process comprises two steps. First, an eye length measurement is performed on the test subject. The peak positions (corresponding to intraocular layers) of the signal curve are determined automatically by a search algorithm, and are displayed on the LabView front panel, starting with the strongest reflecting layer. By selecting any of the peaks, the stepper motor is driven to that position. In the second step, the flip mirror is turned out of the optical path, and the plane $\approx 30$ mm in front of the eye is imaged onto the linear CCD (LCCD) array. The signal from the LCCD is recorded by a PC and displayed in the graphical programming interface LabView. Since the relative movement between the retinal layers and the cornea is smaller than the coherence length, time resolved recording is possible.

## 3 Method

### 3.1 Optical Setup

The optical setup is depicted in Fig. 2. As a light source we use an SLD from Superlum, Russia, with a central wavelength $\lambda$ of 840 nm and an FWHM bandwidth $\Delta\lambda$ of 26.8 nm, resulting in a coherence length $l_c$ of 11.6 $\mu$m (in air). The typical FPA, e.g., the maximum distance change between cornea

and retina, is on the order of 2 to 6 $\mu$m, which is considerably below the coherence length of the light source. Hence, the changes in the interference pattern caused by ocular fundus pulsation are visible as long as the stepper motor is in a position corresponding to an intraocular layer of the subject's eye. The plane $\approx 30$ mm in front of the cornea is imaged via two lenses L1 and L2 onto the APD and the CCD camera ($f_1 = 30$ mm, $f_2 = 80$ mm). By using this setup, L1 is positioned as close to the origin of the interference pattern as possible, so that the losses due to the divergent corneal reflection are minimized.

For the length measurement, the stepper motor is moved at a constant velocity $v$ of 2.88 mm/s, resulting in a Doppler shift $f_D$ of 6840 Hz. The signal from the APD is filtered electronically by a bandpass filter with a central frequency matching $f_D$. After data acquisition, the signal is digitally filtered in LabView. The sensitivity of the system for the length measurement was measured to be 87 dB.

For the observation of fundus pulsations, we used a CCD line camera (Sony ILX551, 2048 pixels, $14 \times 14$-$\mu$m pixel size, 8-bit resolution). Via a pellicle (8R/92T), a small part of the light was guided onto a video camera. Once the subject was correctly positioned—so that the interference fringes could be observed on the video monitor—the signal was recorded with the linear CCD array operated at a line readout rate of 300 to 700 Hz. For the online inspection of the fundus pulsations in LabView, a background subtraction for the elimination of internal reflections and static interference patterns from the subject's eye was performed. For the calculation of the background intensity, a moving average MA($m$) was calculated for each pixel position $m$ using the recursive formula

$$\text{MA}_n(m) = \frac{I(m) + \text{MA}_{n-1}(m) \cdot (N-1)}{N}, \qquad (2)$$

where $I(m)$ is the current intensity of the respective pixel. For $N$, values between 500 and 700 have been chosen. The advantage of this method is the effective removal of static and almost static background signals at a relatively low computational effort, leading to no significant delay in online inspection.

### 3.2 Fringe Contrast

For calculation of fringe contrast, we assumed the radius of curvature of the cornea as 7.8 mm, according to Gullstrand's eye model.[23] Furthermore, we assumed the wave reflected at the anterior corneal surface to be spherical, and the wave reflected at the retina and refracted by the lens and the cornea to be plane. For the following calculation, the distance from the cornea was called $d_z$ (where $z$ is the optical axis) with $d_z = 0$ at the front surface of the cornea, and the distances from the optical axis in $x$ and $y$ directions were called $d_x$ and $d_y$, respectively. The intensity $I$ is then proportional to:

$$I(d_x, d_y, d_z) \propto \left| A \exp(ikd_z) + \frac{0.0078}{r} B \exp(ikr) \right|^2, \quad (3)$$

with $r(d_x, d_y, d_z) = [d_x^2 + d_y^2 + (d_z + 0.0078)^2]^{1/2}$, and $k(\lambda) = 2\pi/\lambda$ ($\lambda = 840 \cdot 10^{-9}$ m). For computation of contrast at a
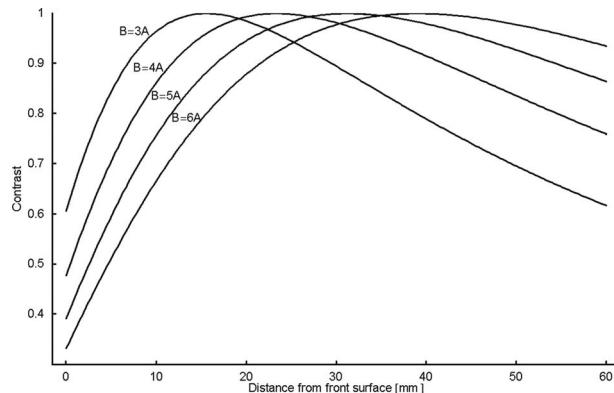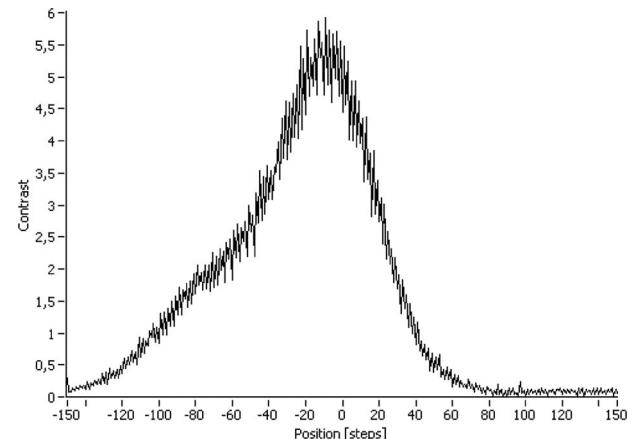
**Fig. 3** Contrast of the fringe system plotted against the distance from the front surface of the cornea and for values of $B/A$ from 3 to 6. $A$ and $B$ are reflection coefficients of the retina and the cornea, respectively.



**Fig. 5** Fringe contrast of an artificial eye plotted against the position of the measurement mirror.

certain position $d_z$, we calculated the intensity at positions of $d_x$ starting from $-1$ to 1 mm in steps of $10^{-3}$ mm and determined the extremes $I_{max}$ and $I_{min}$ of this function. The contrast $C$ is then calculated by:

$$C = \frac{I_{max} - I_{min}}{I_{max} + I_{min}}. \qquad (4)$$

We plotted $C$ for values of $d_z$ from 0 to 60 mm and for values of $B/A$ (reflection coefficient of the cornea in relation to the reflection coefficient of the retina) from 3 to 6 (Fig. 3). The maximum values of $C$ occurred at 15.6 mm ($B/A=3$), 23.4 mm ($B/A=4$), 31.2 mm ($B/A=5$), and 39.0 mm ($B/A=6$), respectively. Experimental results show the maximum contrast between 30 to 40 mm in front of the eye,[13] which suggests a ratio $B/A$ between 5 and 6. For validation of this value, we calculated $B/A$ using the formula for the reflection coefficient $r$ for normal incidence $r=(n_1-n_2)/(n_1+n_2)$, where $n_1$ and $n_2$ are the refractive indices of the first and second medium, respectively, and the refractive indices of the tear film ($n_t=1.336-1.357$[24]), vitreous ($n_v=1.336$[23]), and retina ($n_r=1.4$[25]). We obtained values of $B/A$ between 6.15 and 6.48, in good agreement with our calculations.

When using light of short coherence length, one has to take into account that the fringe contrast also strongly depends on the path length difference of the two reflected beams. The maximum contrast can be observed when this difference matches exactly the optical length of the eye. To study the situation of a slight mismatch in the path length, we observed the interference pattern of an artificial eye for different positions of the stepper motor. This artificial eye consisted of a lens ($f=30$ mm) representing the cornea and a Teflon disk located in the focal plane of the lens representing the retina. For this experiment, the stepper motor was positioned so that the path length difference between the two interferometer arms was 150 steps (37.5 $\mu$m) smaller than the length of the artificial eye. While observing the interference pattern and measuring the contrast, the stepper motor was moved stepwise to a path length difference 37.5 $\mu$m greater than the length of the artificial eye. The use of Eq. (4) for estimation of contrast would overemphasize the influence of single pixels at the two intensity extremes. Thus, in practice it is more useful to take the standard deviation of each line scan as a measure of contrast, which has the advantage of reducing the impact of the readout noise. The synthetic interferogram recorded during these measurements and the contrast curve calculated
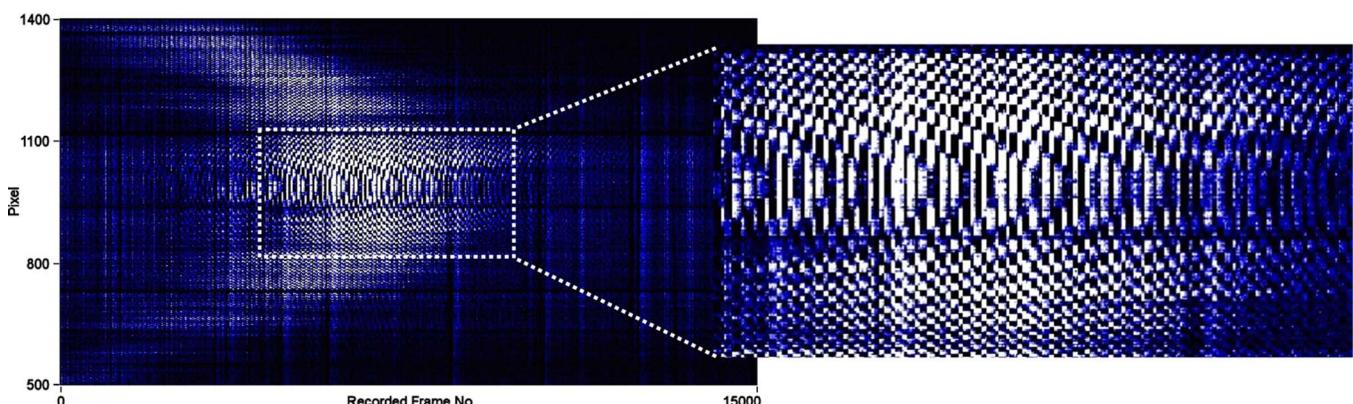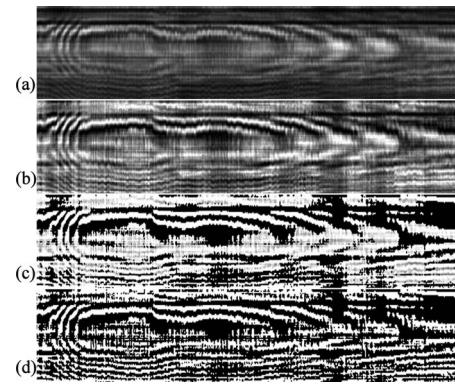


**Fig. 4** Synthetic interferogram recorded from an artificial eye while moving the measurement mirror over a range of 75 $\mu$m around the optical length of the sample.
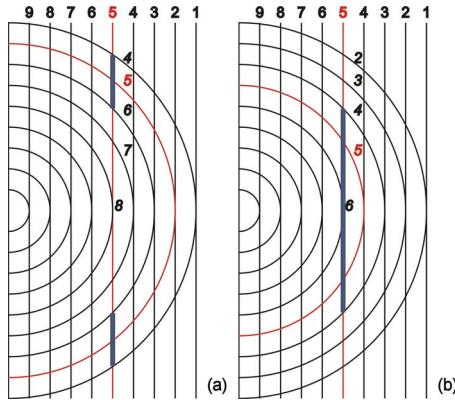
**Fig. 6** Graphical illustration of the localization of the interference contrast. See text for explanation.



**Fig. 7** Steps of image enhancement demonstrated on a synthetic interferogram recorded *in vivo* over one pulse period.

from this dataset are given in Figs. 4 and 5, respectively. As can be seen in Fig. 4, at closer distances of the moving reference mirror the highest intensities occur in the peripheral regions of the fringe system, while at greater distances the maximum intensities are located in the central region. An explanation for this phenomenon can be found by taking a closer look at the interference between plane and spherical wave fronts (Fig. 6). Two reflections of the incident beams generate the interference pattern: the beam coming from the moving mirror is reflected at the anterior surface of the lens representing the cornea and produces a spherical wave, while the beam coming from the fixed mirror is reflected at the Teflon disk representing the retina. The other reflections do not generate visible interference patterns, because the path length difference is not within the coherence length of the light source. If the path length difference between the two mirrors is smaller than the optical length of the eye, the corneal reflection reaches the detection plane earlier than the retinal reflection. In this case, the maximum interference contrast is observed in the outer regions of the synthetic interferogram, which becomes clear when considering that the wave fronts emitted at the same time interfere in the peripheral parts of the fringe system [Fig. 6(a)]. As the path length difference decreases the maximum contrast is shifted toward the center of the fringe system [Fig. 6(b)]. At smaller path length differences, interference fringes can be observed over a wide region in the synthetic interferogram including the center, leading to an increase in contrast. Pixels with constant low intensities, however, reduce the contrast as calculated from the interpixel standard deviation. Thus, the contrast curve in Fig. 5 is asymmetric and its maximum is shifted from the point where the two path lengths are identical by about −10 steps. When the pathway difference matches exactly the length of the eye, the maximum contrast occurs at the center of the fringe system. For obvious reasons if the distance is increased even more, the signal on the CCD is going to zero and the contrast curve drops. The distance range of the stepper motor, in which a signal can be observed in the center of the synthetic interferogram, which corresponds to the maximal observable fundus pulsation amplitude, is approximately 18 $\mu$m. This range is significantly larger than typical FPA values (2 to 6 $\mu$m).[5,13]

In theory, this method would allow for quantification of the eye length, but the current acquisition time is too long for

*in-vivo* application. This, however, could be easily enhanced by a hardware synchronization of the CCD and the stepper motor.

### 3.3 Image Enhancement

The algorithms we use to enhance the visual representation of recorded interferograms are briefly introduced. The main purpose of this process is to achieve an equally distributed intensity, which allows for binarization, and thus, easier analysis of interference fringes.

The first step takes account of the different sensitivities of the CCD pixels as well as local irregularities of the interference patterns, which may originate from internal reflections of the system as well as static interference patterns from the subject's eye and speckle formation. Each "line" of the dataset consists of the signal recorded over time at the same pixel position. For each line, the minimum intensity value $I_{\text{line,min}}$ and the maximum intensity value $I_{\text{line,max}}$ are determined. Furthermore, the global maximum $I_{\text{global,max}}$ of the entire dataset is determined. Then, for every line the minimum is brought to 0 and the maximum to $I_{\text{global,max}}$ by applying the following formula to all data points:

$$I' = (I - I_{\text{line,min}}) \cdot \frac{I_{\text{global,max}}}{I_{\text{line,max}} - I_{\text{line,min}}}. \qquad (5)$$

To reduce the temporal fluctuations of the signal intensity induced by movements of the patient's eye, a similar process is performed for all columns (replacing $I_{\text{line,max}}$ by $I_{\text{col,max}}$ and $I_{\text{line,min}}$ by $I_{\text{col,min}}$ in the previous formula) [see Fig. 7(b)].

The remaining inhomogeneities in the signal intensity are reduced by flat fielding.[26] This is achieved by division of the original data by a low-pass-filtered (blurred) version. The blurred image is created by convolution of the original data with an $8 \times 8$ kernel ($1/64[1 \ldots 1]^{\text{T}}[1 \ldots 1]$, which is equal to averaging over an $8 \times 8$ neighborhood). Before division, all data points of the original image with an intensity lower than 40 to 50% of the maximum intensity are set to 0, while the values of the residual data points remain unchanged. Thus, we avoid low-illuminated areas of the image to become overemphasized. The result of flat fielding can be seen in Fig. 7(c). In the last processing step, a global threshold of 85% with binarization is applied to the image [Fig. 7(d)].
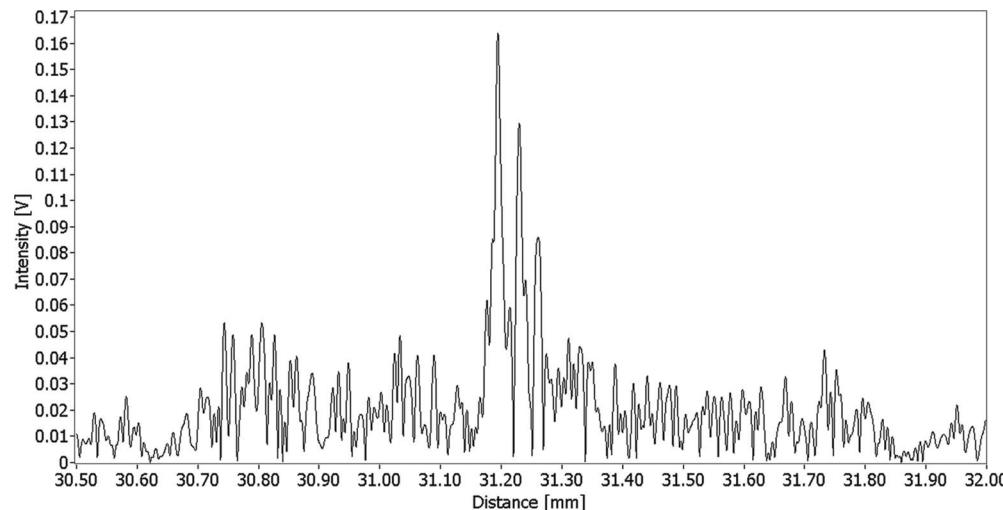
**Fig. 8** Optical A-scan of the posterior segment of a human eye recorded *in vivo* from a healthy volunteer at an angle of 0 deg to the vision axis. The signal peaks indicate the (optical) positions of reflecting interfaces.

### 3.4   In-Vivo Measurements

Preliminary measurements were performed on young emmetropic subjects at two different angles of vision. The signal peaks in the length measurements represent the positions of several retinal layers.

The first measurements were performed at an angle of 0 deg with respect to the vision axis. Two peaks, the first one at 31.20 mm (with respect to equal interferometer arm length) probably corresponding to the retinal pigment epithelium (RPE) or Bruch's membrane, the other at 31.25 mm to choroidal structures (Fig. 8), were chosen for measurement of fundus pulsations. These peaks were easily reproducible in almost all length measurements, while the inner limiting membrane (ILM) is in most cases not observable at 0 deg. The synthetic interferograms were recorded at the corresponding stepper motor positions [Figs. 9(a) and 9(b)] at a frequency of 600 Hz. The images representing fundus pulsation data were enhanced by the algorithms explained in the previous chapter; the last thresholding step was performed without binarization. The average length of a pulse period was approximately 1.08 s, and the average fundus pulsation amplitude was 1.7 $\mu$m. Schmetterer and Wolzt have shown that the time course of the fundus pulsation is in very good agreement with the time course of the integrated velocity curve in the posterior ciliary arteries.[5] Hence, assuming a nonpulsatile venous outflow, the duration in which the distance between the anterior corneal surface and the posterior pole of the eye decreases corresponds to the duration of choroidal engorgement during the cardiac cycle. By averaging over the presented pulse periods, we obtained a value of 133 ms for the described process.

For the second measurements we chose an angle of ~7 deg nasal to the vision axis and, for better identification of retinal structures, averaged ten consecutive A-scans (Fig. 10). The observed signal peaks can be assigned to the retinal layers in the following way.[20] Peak 1 (31.00 mm) is most probably caused by light reflected at the ILM, and peak 4 (31.34 mm) by a reflection at the RPE or Bruch's membrane. We assume that peak 3 can be assigned to the retinal nerve fiber layer, and peaks 5 and 6 to choroidal structures. We measured the fundus pulsation at stepper motor positions corresponding to peaks 1 and 4 [Figs. 11(a) and 11(b)]. We found an average length of a pulse period of 0.95 s, and an average fundus pulsation amplitude of 2 $\mu$m. The duration of choroidal engorgement was 350 ms for this subject.

Fundus pulsations occurred only at positions that were related to signal peaks in the length measurements, and disappeared when moving the stepper motor out of the coherence gate. At both angles of vision, we found no significant difference in the fundus pulsation amplitudes of the (neighboring) retinal layers, as expected for healthy subjects.

## 4   Conclusion

We describe a method called LCTI, which allows for the measurement of fundus pulsations at preselected layers of the ocular fundus. This is feasible as long as the distance of the respective layers can be resolved with the incorporated PCI, and as long as the movement of the retinal layer does not largely exceed the coherence length of the light source. Using this approach, we were able to study the relative movement between the front surface of the cornea and several preselected retinal layers.

With some extension the applications of this system may be wide. In humans it may be difficult to measure the relative movement of the anterior surface of the cornea and the submacular sclera, because of the high blood volume within the choroid and the associated scattering and absorption. In experimental animals, however, a scleral peak can easily be observed.[27] Real-time measurement of distance changes between cornea and sclera may have two important applications. On the one hand it may be possible to measure real-time growth of axial eye length in myopia models. Although this would require quite long measurement times of several hours, such measurements seem feasible because the increase in axial eye length in one-year-old chicken is approximately 6 $\mu$m per day,[28] which should easily be detectable with the

(a)



(b)
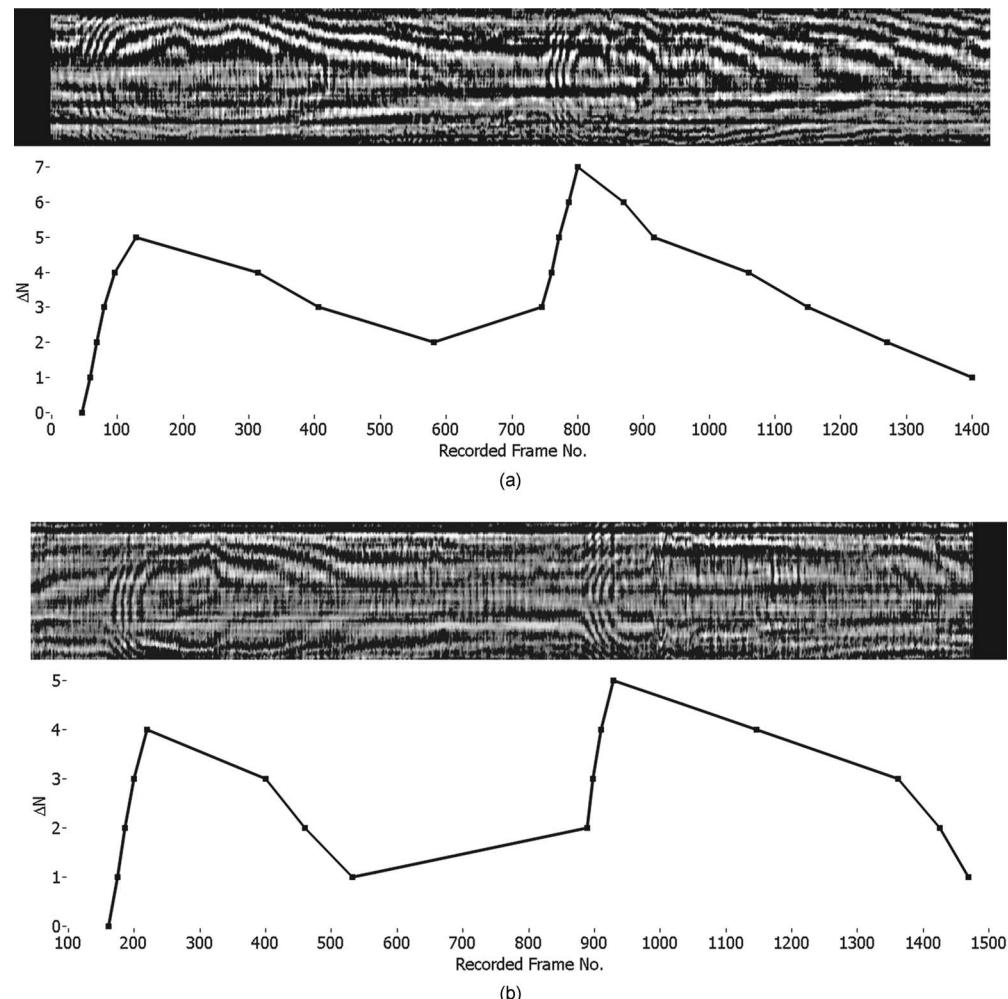
**Fig. 9** (a) and (b) Synthetic interferograms recorded *in vivo* at a frequency of 600 Hz and at an angle of 0 deg to the vision axis from a healthy volunteer over two pulse periods at the two strongest reflecting layers in Fig. 8 (31.20 and 31.25 mm) and contraction-dilatation graph (time course of the distance between cornea and the respective layer).
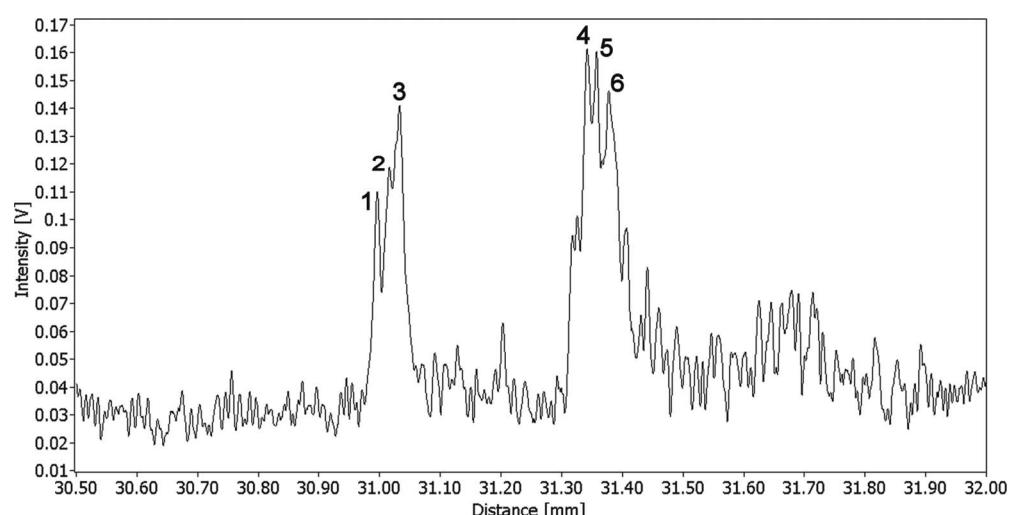


**Fig. 10** Optical A-scan of the posterior segment of a human eye recorded *in vivo* from a healthy volunteer at an angle of ∼7 deg nasal to the vision axis. The signal peaks indicate the (optical) positions of reflecting interfaces.
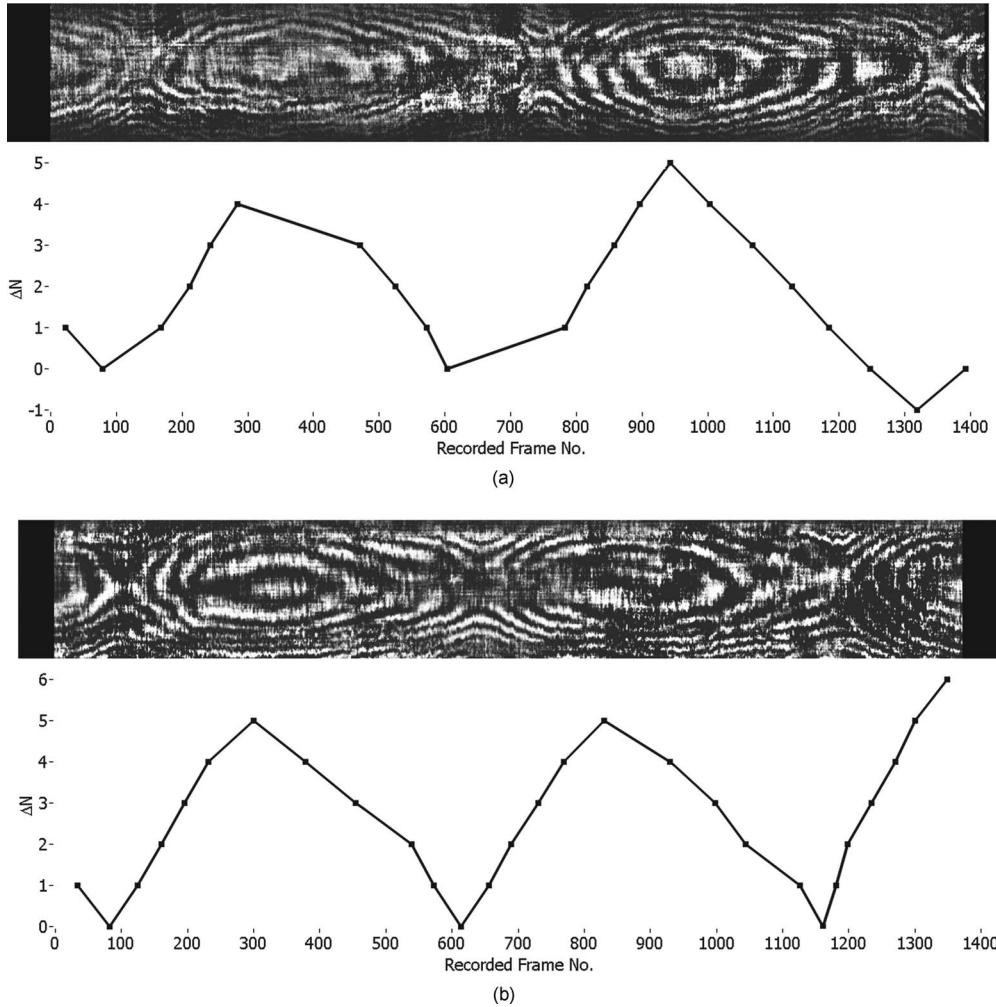
**Fig. 11** (a) and (b) Synthetic interferograms recorded *in vivo* at a frequency of 600 Hz and at an angle of ~7 deg nasal to the vision axis from a healthy volunteer over two pulse periods at two reflecting layers in Fig. 10 (31.00 and 31.34 mm, which correspond to peaks 1 and 4, respectively) and contraction-dilatation graph.

present LCTI providing a resolution of less than 0.4 $\mu$m ($\lambda/2$).

On the other hand, LCTI may also be used to gain insight into pulsatile ocular blood flow. We have previously provided a mathematical model to relate fundus pulsation to POBF, but this model was based on conventional FPA measurements only. Nevertheless, this model showed POBF values that were close to data obtained by other techniques. Obviously, real-time measurement of corneo-scleral distance may provide a much more reliable measure to calculate ocular volume changes associated with pulsatile inflow of blood into ocular vessels.

Although LCTI in human subjects is limited to the investigation of retinal layers and choroidal structures, it could also be used in clinical studies of human ocular pathologies. Contrary to healthy subjects, where the different retinal layers are moving in parallel, in pathologic cases, e.g., in patients with macular edema, such a parallel movement may not be expected.

One could argue that a frequency domain optical coherence tomography (FDOCT) system could be applied for the analysis of fundus pulsations, which would have the advantage of a higher sensitivity of the length measurement compared to our system and the ability of transversal scanning. However, the axial resolution of FDOCT systems is limited to the order of the coherence length, which is not sufficient for the (time-resolved) measurement of fundus pulsations. A phase-resolved measurement would only be possible for short time spans, since the phase information is destroyed by even very small movements of the eye. Furthermore, the phase noise would become problematic when adding up the phase information over a longer period of time. In current OCT systems, the phase difference between adjacent A-scans is utilized to gain information about the velocity of moving scatterers.[29,30] However, due to the previously mentioned reasons it presently seems not feasible to obtain stable phase information *in vivo* over a longer time, especially when using a transversal scanner, which would make it necessary to compare the phase values of temporally separated A-scans. Furthermore, the amount of data generated by this method is too large to be recorded over a time of more than a few seconds.

In conclusion we present a new technique capable of measuring distance changes between preselected ocular surfaces. Here, we present heart-rate-related distance changes between

the cornea and different reflecting layers, including ILM and Bruch's membrane, in healthy subjects. The applications of this technology may be, however, much wider, including the study of eye elongation in myopia models and the study of ocular blood flow by measuring pulse-related changes in ocular volume.

## Acknowledgment

## References

1. O. Findl, G. Rainer, S. Dallinger, G. Dorner, K. Polak, B. Kiss, M. Georgopoulos, C. Vass, and L. Schmetterer, "Assessment of optic disk blood flow in patients with open-angle glaucoma," *Am. J. Ophthalmol.* **130**, 589–596 (2000).
2. L. Schmetterer, A. Kruger, O. Findl, H. Breiteneder, H. G. Eichler, and M. Wolzt, "Topical fundus pulsation measurements in age-related macular degeneration," *Graefe's Arch. Clin. Exp. Ophthalmol.* **236**, 160–163 (1998).
3. L. Schmetterer and M. Wolzt, "Ocular blood flow and associated functional deviations in diabetic retinopathy," *Diabetologia* **42**, 387–405 (1999).
4. K. Polak, E. Polska, A. Luksch, G. Dorner, G. Fuchsjäger-Mayrl, O. Findl, H. G. Eichler, M. Wolzt, and L. Schmetterer, "Choroidal blood flow and arterial blood pressure," *Eye* **17**, 84–88 (2003).
5. L. Schmetterer and M. Wolzt, "Laser interferometric investigations of pulsatile choroidal blood flow: review and new results on the validity of the technique," *J. Biomed. Opt.* **3**(3), 246–252 (1998).
6. L. Schmetterer and G. Garhöfer, "How can blood flow be measured?" *Surv. Ophthalmol.* **52**(Suppl 2), S134–138 (2007).
7. A. Hommer, G. Fuchsjäger-Mayrl, H. Resch, C. Vass, G. Garhöfer, and L. Schmetterer, "Estimation of ocular rigidity based on measurement of pulse amplitude using pneumotonometry and fundus pulse using laser interferometry in glaucoma," *Invest. Ophthalmol. Visual Sci.* **49**, 4046–4050 (2008).
8. A. Harris, H. S. Chung, T. A. Ciulla, and L. Kagemann, "Progress in measurement of ocular blood flow and relevance to our understanding of glaucoma and age-related macular degeneration," *Prog. Retin Eye Res.* **18**, 669–687 (1999).
9. C. E. Riva, S. D. Cranstoun, J. E. Grunwald, and B. L. Petrig, "Choroidal blood flow in the foveal region of the human ocular fundus," *Invest. Ophthalmol. Visual Sci.* **35**, 4273–4281 (1994).
10. D. M. Silver and R. A. Farrell, "Validity of pulsatile ocular blood flow measurements," *Surv. Ophthalmol.* **38**(Suppl), S72–80 (1994).
11. W. E. Lieb, S. M. Cohen, D. A. Merton, J. A. Shields, D. G. Mitchell, and B. B. Goldberg, "Color Doppler imaging of the eye and the orbit," *Arch. Ophthalmol. (Chicago)* **109**, 527–531 (1991).
12. A. F. Fercher, "In vivo measurement of fundus pulsations by laser interferometry," *IEEE J. Quantum Electron.* **20**, 1469–1471 (1984).
13. L. Schmetterer, F. Lexer, C. Unfried, H. Sattmann, and A. F. Fercher, "Topical measurement of fundus pulsations," *Opt. Eng.* **34**(3), 711–716 (1995).
14. B. Kiss, S. Dallinger, K. Polak, O. Findl, H. G. Eichler, and L. Schmetterer, "Ocular hemodynamics during isometric exercise," *Microvasc. Res.* **61**, 1–13 (2001).
15. L. Schmetterer, S. Dallinger, O. Findl, H. G. Eichler, and M. Wolzt, "A comparison between laser interferometric measurement of fundus pulsation and pneumotonometric measurement of pulsatile ocular blood flow. 1. Baseline considerations," *Eye* **14**, 39–45 (2000).
16. L. Schmetterer, S. Dallinger, O. Findl, U. Graselli, H. G. Eichler, and M. Wolzt, "A comparison between laser interferometric measurement of fundus pulsation and pneumotonometric measurement of pulsatile ocular blood flow. 2. Effects of changes in $pCO_2$ and $pO_2$ and of isoproterenol," *Eye* **14**, 46–52 (2000).
17. C. K. Hitzenberger, "Optical measurement of the axial eye length by laser Doppler interferometry," *Invest. Ophthalmol. Visual Sci.* **32**, 616–624 (1991).
18. C. K. Hitzenberger, "Measurement of corneal thickness by low-coherence interferometry," *Appl. Opt.* **31**, 6637–6642 (1992).
19. W. Drexler, C. K. Hitzenberger, H. Sattmann, and A. F. Fercher, "Measurement of the thickness of fundus layers by partial coherence tomography," *Opt. Eng.* **34**(3), 701–710 (1995).
20. C. K. Hitzenberger, W. Drexler, A. Baumgartner, F. Lexer, H. Sattmann, M. Esslinger, M. Kulhavy, and A. F. Fercher, "Optical measurement of intraocular distances: a comparison of methods," *Lasers Light* **8**, 85–95 (1997).
21. A. F. Fercher and E. Roth, "Ophthalmic laser interferometry," *Proc. SPIE* **658**, 48–51 (1986).
22. A. F. Fercher, K. Mengedoht, and W. Werner, "Eye length measurements by interferometry with partially coherent light," *Opt. Lett.* **13**, 186–189 (1988).
23. A. Gullstrand, "The dioptrics of the eye," in *Helmholtz's Treatise on Physiological Optics*, J. P. C. Southall, Ed., Vol. **1**, pp. 351–352, Optical Society of America, Washington, D.C. (1924).
24. S. Patel, J. Marshall, and F. W. Fitzke 3rd, "Refractive index of the human corneal epithelium and stroma," *J. Refract. Surg.* **11**, 100–105 (1995).
25. M. G. Wirtitsch, E. Ergun, B. Hermann, A. Unterhuber, M. Stur, C. Scholda, H. Sattmann, T. H. Ko, J. G. Fujimoto, and W. Drexler, "Ultrahigh resolution optical coherence tomography in macular dystrophy," *Am. J. Ophthalmol.* **140**, 976–983 (2005).
26. M. Seul, L. O'Gorman, and M. J. Sammon, "Edge enhancement and flat fielding," Chap. 3.3. in *Practical Algorithms for Image Analysis*, pp. 75–79, Cambridge University Press, Cambridge, UK (2000).
27. G. F. Schmid, G. I. Papastergiou, D. L. Nickla, C. E. Riva, T. Lin, R. A. Stone, and A. M. Laties, "Validation of laser Doppler interferometric measurements in vivo of axial eye length and thickness of fundus layers in chicks," *Curr. Eye Res.* **15**, 691–696 (1996).
28. G. I. Papastergiou, G. F. Schmid, C. E. Riva, M. J. Mendel, R. A. Stone, and A. M. Laties, "Ocular axial length and choroidal thickness in newly hatched chicks and one-year-old chickens fluctuate in a diurnal pattern that is influenced by visual experience and intraocular pressure changes," *Exp. Eye Res.* **66**, 195–205 (1998).
29. R. M. Werkmeister, N. Dragostinoff, M. Pircher, E. Götzinger, C. K. Hitzenberger, R. A. Leitgeb, and L. Schmetterer, "Bidirectional Doppler Fourier-domain optical coherence tomography for measurement of absolute flow velocities in human retinal vessels," *Opt. Lett.* **33**, 2967–2969 (2008).
30. R. A. Leitgeb, L. Schmetterer, F. Berisha, C. K. Hitzenberger, M. Wojtkowski, T. Bajraszewski, and A. F. Fercher, "Real-time measurement of in vitro flow by Fourier-domain color Doppler optical coherence tomography," *Opt. Lett.* **29**, 171–173 (2004).